Available online at www.sciencedirect.com
SCIENCE DIRECT®
International Journal of Multiphase Flow 31 (2005) 618–642
International Journal of Multiphase Flow
www.elsevier.com/locate/ijmulflow

Visualization of boiling phenomena in inclined rectangular gap

Y.H. Kim [a], S.J. Kim [a], J.J. Kim [a], S.W. Noh [a], K.Y. Suh [a,*], J.L. Rempe [b], F.B. Cheung [c], S.B. Kim [d]

[a] *Department of Nuclear Engineering, Seoul National University, San 56-1 Sillim-dong, Gwanak-gu, Seoul 151-742, Republic of Korea*
[b] *Idaho National Engineering & Environmental Laboratory, Idaho Falls, ID 83415, USA*
[c] *Pennsylvania State University, University Park, PA 16802, USA*
[d] *Korea Atomic Energy Research Institute, Yuseong, Daejeon 305-600, Republic of Korea*

Received 6 May 2004; received in revised form 11 January 2005

Abstract

An experimental study was performed to investigate the pool boiling critical heat flux (CHF) in one-dimensional inclined rectangular channels by changing the orientation of a copper test heater assembly. In a pool of saturated water under the atmospheric pressure, the test parameters included the gap sizes of 1, 2, 5, and 10 mm, and the surface orientation angles from the downward-facing position (180°) to the vertical position (90°). Tests were conducted on the basis of the visualization of boiling phenomena in the narrowly confined channel and open periphery utilizing a high-speed digital camera. To prevent the heat loss from the water pool and copper test heater, a state-of-the-art vacuum pumping technique was introduced. It was observed that the CHF generally decreased as the surface inclination angle increased and as the gap size decreased. In the downward-facing position (180°), however, the vapor movement was enhanced by the gap structure, which produced the opposing result; that is, the CHF increased as the gap size decreased. Phenomenological characteristics regarding the interfacial instability of vapor layer were addressed in terms of visualization approaching the CHF. It was found that there exists a transition angle, around which the CHF changes with a rapid slope.

* Corresponding author. Tel.: +82 2 880 8324; fax: +82 2 889 2688.
E-mail address: kysuh@snu.ac.kr (K.Y. Suh).

0301-9322/$ - see front matter © 2005 Elsevier Ltd. All rights reserved.
doi:10.1016/j.ijmultiphaseflow.2005.01.002

Keywords: Critical heat flux; Gap size effect; Surface orientation effect; Transition angle; Interfacial instability; Rectangular gap

1. Introduction

A great deal of literature exists relating to the effect of surface orientation and gap size on the pool boiling heat transfer and critical heat flux (CHF) characteristics. The engineered results are applied to cooling of the electronic and power appliances, heat treatment of the metallic parts, and cooling of the superconductor coils. In view of nuclear reactor safety management, it is crucial to accurately predict the CHF and phenomenological boiling dynamics (Kim and Suh, 2000a,b; Yoon and Suh, 2000; Cho et al., 2000, 2004; Lee and Suh, 2003; Rempe et al., 2004a,b, 2003; Dizon et al., 2004; Cheung et al., 2004; Knudson et al., 2004). In the Three-Mile Island Unit 2 (TMI-2) accident, for instance, the lower part of the reactor vessel was overheated but then rather rapidly cooled down (Wolf and Rempe, 1993; Henry and Fauske, 1993; Suh and Henry, 1996a,b; Rempe et al., 2001). It was suggested that this rapid cooldown may have been due to cooling in a narrow gap, smaller than the order of centimeters, which may have formed between the solidified core debris and the reactor vessel lower head. To better quantify such cooling, experiments are being conducted to quantify the CHF associated with bubble behavior that may affect the entire state of the heat transfer mode. Various two-phase flow patterns are also observed to gain insights about the fundamental physics required to interpret the data. In this sense, one needs to design the CHF test sections to simulate both the confined and angle convertible channels.

Heretofore, a great deal of experimental studies have been reported concerning the heater surface orientation (Ishigai et al., 1961; Githinji and Sabersky, 1963; Nishikawa et al., 1984), in which several researchers have tried to interpret the CHF mechanism for pool boiling by correlating the CHF data into a generalized equation (Brusstar and Merte, 1994; Brusstar et al., 1997; Chang and You, 1996; El-Genk and Guo, 1993; Guo and El-Genk, 1992; Howard and Mudawar, 1999; Vishnev, 1974) and for flow boiling circumstance (Galloway and Mudawar, 1993; Gersey and Mudawar, 1995). Among them, El-Genk and Guo (1993) developed the following CHF correlation for water that considers orientation

$$q_{\mathrm{CHF}} = [0.034 + 0.0037(180 - \theta)^{0.656}]\rho_{\mathrm{G}} h_{\mathrm{LG}} [\sigma(\rho_{\mathrm{L}} - \rho_{\mathrm{G}})g/\rho_{\mathrm{G}}^2]^{0.25} \tag{1}$$

where q_{CHF} is the CHF in W/m^2, ρ_{L} and ρ_{G} are the saturated liquid and vapor densities in kg/m^3, h_{LG} is the latent heat of vaporization in J/kg, σ is the surface tension, g is the gravitational acceleration in m/s^2, and θ is the heater surface orientation angle in degrees. The function of angle θ varies with the working fluid. The correlation of other investigators (Vishnev, 1974; Brusstar and Merte, 1994; Brusstar et al., 1997) takes on a similar form. Recently, some researchers mentioned the existence of a transition angle at which the CHF decreases rapidly (Howard and Mudawar, 1999; Yang et al., 1997).

Also many investigators have attempted to predict the gap size effect on the CHF in various channels. Several correlations were generated in terms of the predominant functional variables (Chang and Yao, 1983; Chyu, 1988; Katto and Kosho, 1979; Kim et al., 2000; Monde et al., 1982). With the aid of dimensional analysis developed by Katto (1978), the following correlating

equation can be obtained for the CHF during natural convective boiling in confined channels in the near-vertical region

$$\frac{q_{\mathrm{CHF}}/\rho_{\mathrm{G}}h_{\mathrm{LG}}}{\sqrt[4]{\sigma g\sin(\theta)(\rho_{\mathrm{L}}-\rho_{\mathrm{G}})/\rho_{\mathrm{G}}^2}}=\frac{C_1}{1+C_2(\rho_{\mathrm{L}}/\rho_{\mathrm{G}})^{C_3}(g\sin(\theta)(\rho_{\mathrm{L}}-\rho_{\mathrm{G}})s^2/\sigma)^{C_4}(D_{\mathrm{h}}/s)} \tag{2}$$

where ρ_{L} and ρ_{G} are the saturated liquid and vapor density, h_{LG} is the latent heat of vaporization, g is the gravitational acceleration, θ is the heater surface orientation angle, σ is the surface tension, C_1 is the constant, C_2 is the coefficient, C_3 and C_4 are exponents, s is the channel gap size, and $D_{\mathrm{h}}=2wl/(w+l)$ is the equivalent heated surface diameter, in which w and l refer to the width and length of the heated channel.

Monde et al. (1982) conducted the CHF experiments with a copper plate in the vertical rectangular channel with gap sizes ranging from 0.45 to 7.00 mm. They correlated their CHF data with corresponding l/s being less than 120 in four test liquids: water, ethanol, R-113, and benzene within 20% as

$$\frac{q_{\mathrm{CHF}}/\rho_{\mathrm{G}}h_{\mathrm{LG}}}{\sqrt[4]{\sigma g(\rho_{\mathrm{L}}-\rho_{\mathrm{G}})/\rho_{\mathrm{G}}^2}}=\frac{0.16}{1+6.7\times10^{-4}(\rho_{\mathrm{L}}/\rho_{\mathrm{G}})^{0.6}(l/s)} \tag{3}$$

where ρ_{L} and ρ_{G} are the saturated liquid and vapor density, h_{LG} is the latent heat of vaporization, σ is the surface tension, g is the gravitational acceleration and l and s denote heater length and gap size, respectively.

The CHF triggering mechanism yet defies full understanding primarily due to the complexity of the effect of surface inclination and gap size. Hence, the current study was performed to predict the CHF in confined channels by varying the gap size and orientating the test specimen. Results were obtained in the vicinity of the CHF as well as in the nucleate boiling regime utilizing the GAMMA (Gap Apparatus Mitigating Melt Attack) apparatus at the Seoul National University.

2. Experiment

2.1. Experimental apparatus and conditions

The experimental apparatus was heated by supplying DC power of 6 kW with DC output of 300 V and current of 20 A. The signals from the output voltage, ampere and watt generated on the test heater material were exported by RS-232C to the IBM PC communication. A quasi-direct heating method was adopted to generate sufficient heat flux in the testing. The power lead contact area on the test heater can drastically be reduced by silver-soldering the high resistance thin film resistor underneath the test heater.

A heater assembly was fabricated utilizing a copper block test heater and a thin film resistor, which were designed first to facilitate use of the state-of-the-art devices for visualization of the vapor behavior, and second to avoid use of direct current capacity exceeding 10 A. A copper block belonging to the heater assembly had the wetted surface of 15×35 mm^2 in width by length, to which a thin film resistor having a resistance of 20 Ω was affixed. A schematic diagram of the copper block heater is illustrated in Fig. 1, where three chromel–alumel (K-type) thermocouples

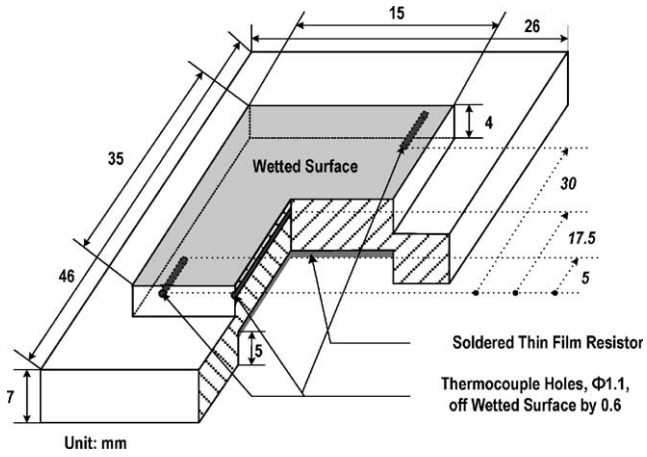

Fig. 1. Schematic diagram of test heater block.

for measuring the temperature data on the wetted surface were inserted into the hole off the wetted surface by 0.6 mm and the depths of 5, 17.5 and 30 mm in the direction of the flow channel, respectively. Essentially, the test heater was slightly coated with nickel to prevent the test heater from being oxidized.

Regarding the device holding the heater assembly, the stainless steel housing was designed to ensure the most effective insulation on the heated section, as illustrated in Fig. 2. In order to efficiently insulate the heated section, the interior of the housing is evacuated, and the inner surface of the housing is polished smoothly to increase the efficiency of vacuum insulation. The insulation efficiency is surprisingly high for vacuums of 10^{-4} Torr, and such vacuums sizably reduce the heat loss from the bottom of the copper block heater. Pyrex glass was imbedded into the edge of the housing and designed to precisely maintain the gap sizes of 1, 2, 5 and 10 mm, and to visualize the test apparatus having a narrow rectangular channel, as demonstrated in Fig. 2. Without the Pyrex

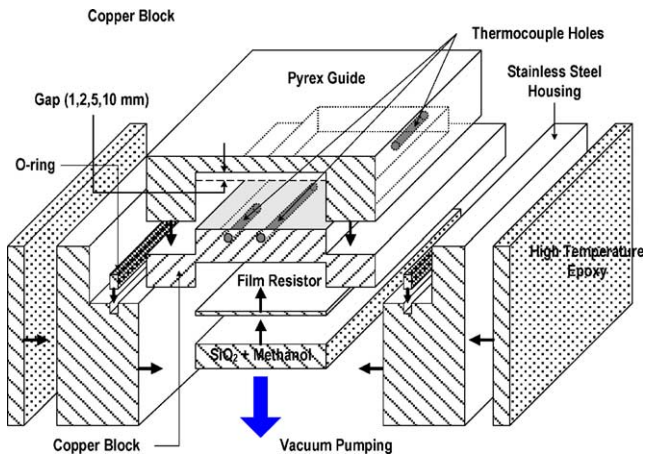

Fig. 2. Cross-sectional view of test heater assembly (gap sizes: 1, 2, 5 and 10 mm).

guide, Fig. 3 shows the same structure of the heater assembly for pool boiling in an open periphery experiment.

In the same way as the housing, the water pool shown in Figs. 4 and 5 was evacuated for the purpose of insulation. Two stainless steel tanks constitute water pool and the space between those could be evacuated by vacuum pumping. Hence, this functioned to sustain a steady thermodynamic state of water at the atmospheric pressure, in which eight immersion type heaters having the electric capacity of 2 kW were homogeneously inserted into the test pool to pre-heat the de-mineralized water in the test pool up to the saturated state. A reflux condenser was equipped in the test pool itself to maintain the pressure in the water pool.

After the experimental apparatus had fully been installed, the CHF was measured in the narrow channel of the crevice type copper heater block at predetermined inclination angles under the atmospheric pressure in the water pool. The temperature data were read from the six K-type thermocouples for the bulk fluid utilizing the computer based data acquisition system mainframe of HP VXI-E8406A functioned with the module of HP-1413C. The saturated water temperature in the vacuum pool was precisely controlled with two temperature controllers. The temperature readings were ten times per second, whose information was filed in a text file by the HP-VEE 5.0 measurement software.

2.2. Experimental procedure and data reduction

The experimental procedure is explained below (see Fig. 6). First, the heater surface was cleaned with acetone prior to each test. The pool was deaerated by running the immersion-type heaters at the atmospheric saturated boiling condition for at least an hour prior to reading the data. Although this study is focused on the quantitative investigation of the CHF, data in the nucleate boiling regime prior to reaching the CHF were also obtained.

Maintaining the thermodynamically saturated condition at atmospheric pressure, the heat flux was gradually increased utilizing a direct power supply. At each stage, vapor behavior in the confined channels and open periphery was photographed through the view port using a high-speed digital camera at 4000 fps, in which several high capacity light sources provided illumination

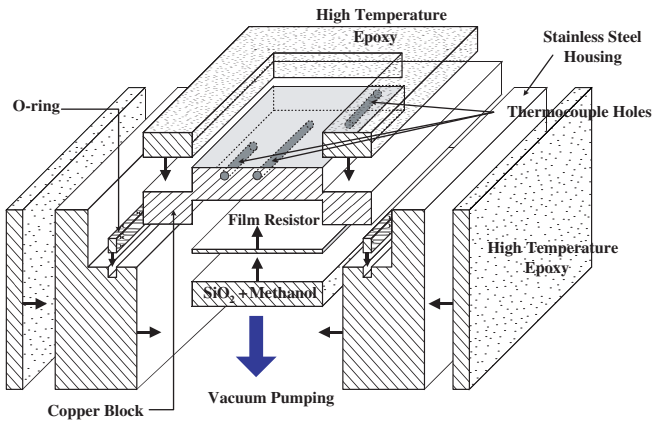

Fig. 3. Cross-sectional view of test heater assembly (open periphery).

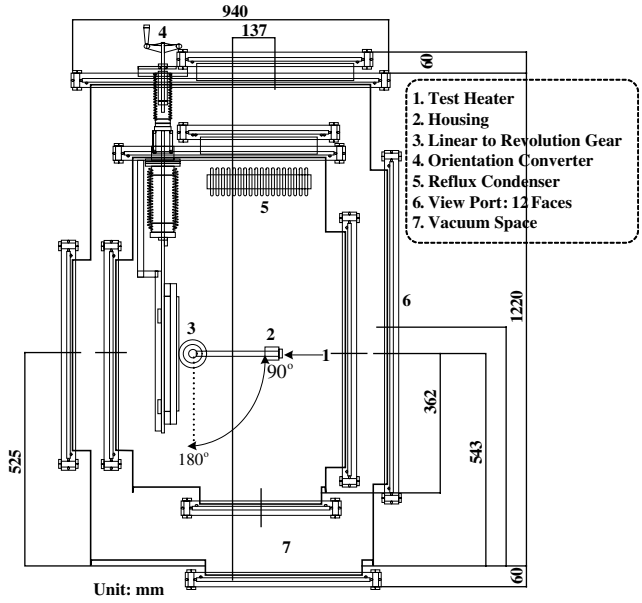

Fig. 4. Front view of vacuum water pool.

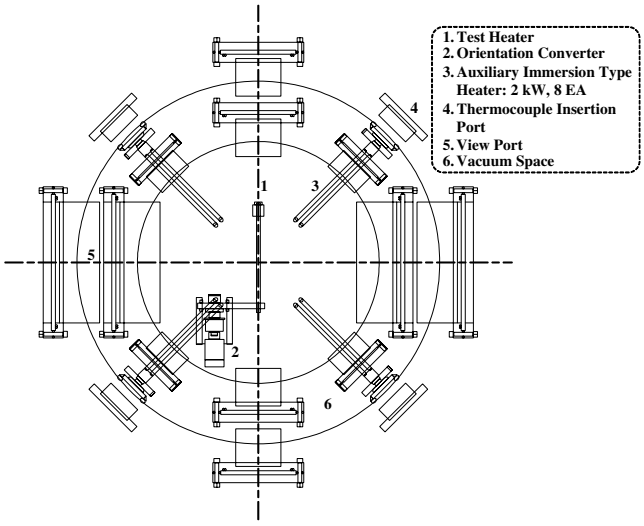

Fig. 5. Top view of vacuum water pool.

for the high-speed photography. Together with visualization, the heated surface temperature was monitored using HP VEE5.0 and stored in data file format. While monitoring the temperature, the CHF was judged to occur when the surface temperature rose in a rapid slope. The temperature jumps were detected in the range from 0.75 to 5 K/s at the constant DC power when the CHF was reached. The CHF was determined as the highest average heat flux that gave a stable temperature reading plus one half of the last average power increment (~3% of the CHF). In order to protect

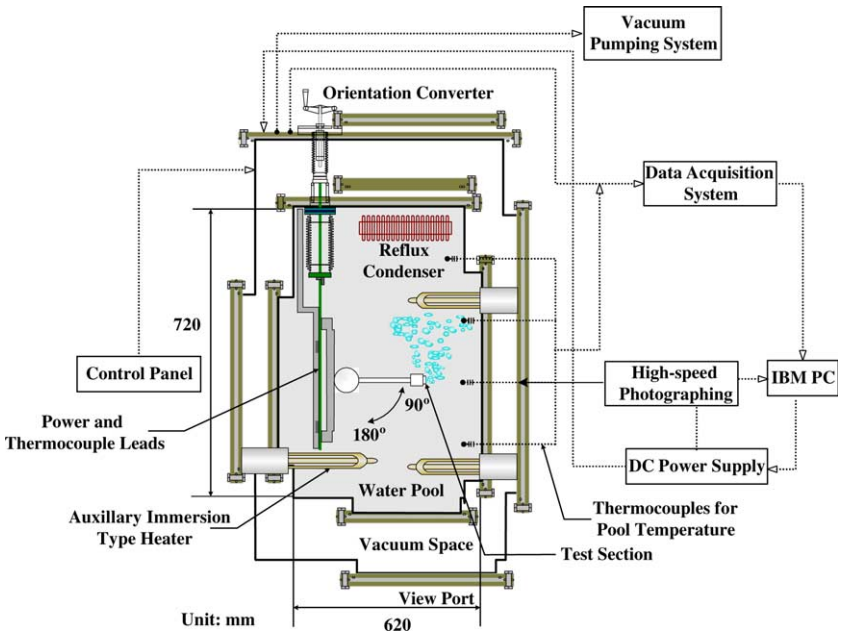

Fig. 6. Schematic diagram of GAMMA test apparatus.

the thin film resistor from burnout, the electrical power was turned off immediately after the surface temperature had reached 190 °C.

After appropriate analysis of the heat flux and temperature data, the CHF values were determined for all the surface orientation angles within ±5%. In calculating the uncertainties associated with the experimental data readings, a quadratic method of error propagation was utilized, in which the fractional uncertainties are added in quadrature (Taylor, 1982). The K-type thermocouples were calibrated for a maximum uncertainty of ±0.1 °C. The uncertainty in the heat flux due to instrumentation limitations was estimated to be 1%. As mentioned earlier, this study adopted the vacuum pumping method to prevent the heat loss from the sides other than that adjacent to the working fluid. Radiation heat transfer to the opposite direction of the heater is negligible because the interior of housing is in vacuum. Conduction heat loss between the copper block and the housing was minimized by attaching a high temperature epoxy alongside the periphery of the housing. In the experiment, no bubbles were observed in the periphery of the housing. Hence, the heat loss was considered to be negligible enough to ascertain full energy transfer from the heated surface to the working fluid.

3. Experimental results

3.1. Pool and gap boiling visualization in inclined downward- and upward-facing region

Fundamental characteristics of the pool boiling environment can be extended to understand gap boiling. Hence, in order to understand the interrelation between the two kinds of boiling states, this study used a one-dimensional test heater assembly with and without the gap structure.

Figs. 7 and 8 demonstrate the typical pool boiling phenomena at inclined upward and downward locations, i.e. 45° and 135°, respectively. In addition, Fig. 9 presents the narrow gap boiling bubble behavior in terms of the heat flux reaching the CHF at the same circumstances for the confined channel of 5 mm gap.

Comparing Figs. 7 and 8, the former figure suggests that the free escape of vapor from the wetted surface of the test heater is driven by buoyancy rather than convection, whereas the latter figure suggests that the movement of bubbles is restricted by geometrical location due to gravity (e.g., bubbles are momentarily taken off the surface by the momentum of vapor generation and then escape from the region of the heated surface by buoyancy). For this reason, the approximate bubble diameter and overall size in the upward location are slightly larger than those in the downward location. On the other hand, most of the bubble growth and departure in Fig. 9 is related to the competing gravitational and buoyant forces. This apparently explains the physical role of the gap structure, which can give an essential clue for improving the insightful analysis of the pool and gap boiling phenomena. Compared to phenomena observed for pool boiling, confined channel bubble growth and coalescence are primarily due to the gap size effect associated with the gravitational and buoyant forces. In the vicinity of CHF, a stable vapor film is maintained, which results in sudden temperature escalation at the heated surface and finally, CHF.

In particular, the vapor layer thickness normal to the heated surface in the open periphery is larger than that in the 5 mm gap. This larger vapor film and free escaping vapor from the heater surface may explain the increased resistance against thermal attack at the heat removal surface. Accordingly, the CHF in the open periphery is larger than that in the 5 mm gap at a given surface inclination angle (Kim and Suh, 2003). Considering interrelation between the CHF and the heat transfer coefficient, however, this is not always directly related to larger heat transfer coefficient in

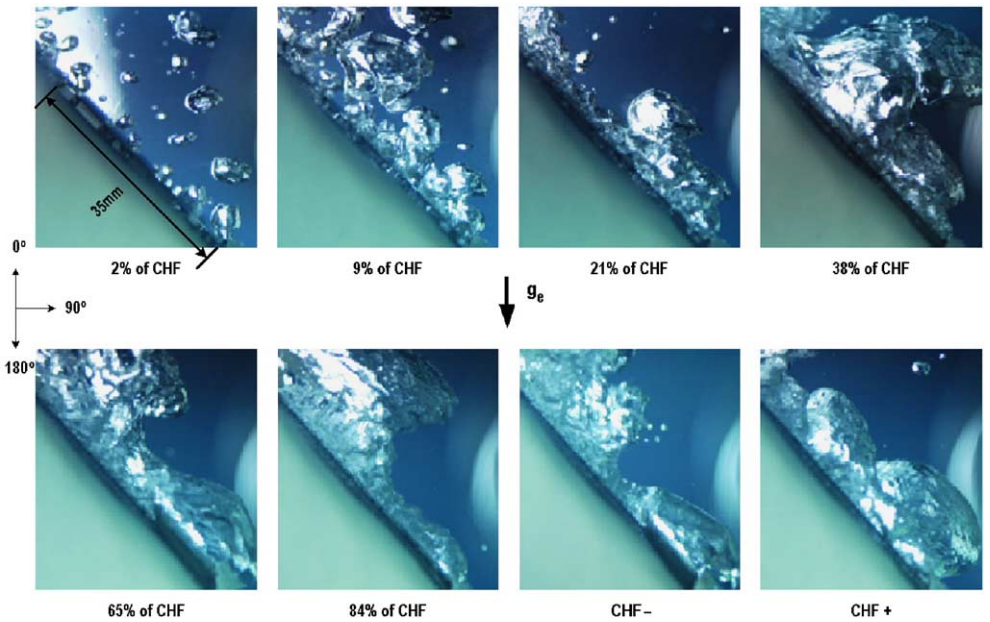

Fig. 7. Flow visualization (open periphery, 45°).

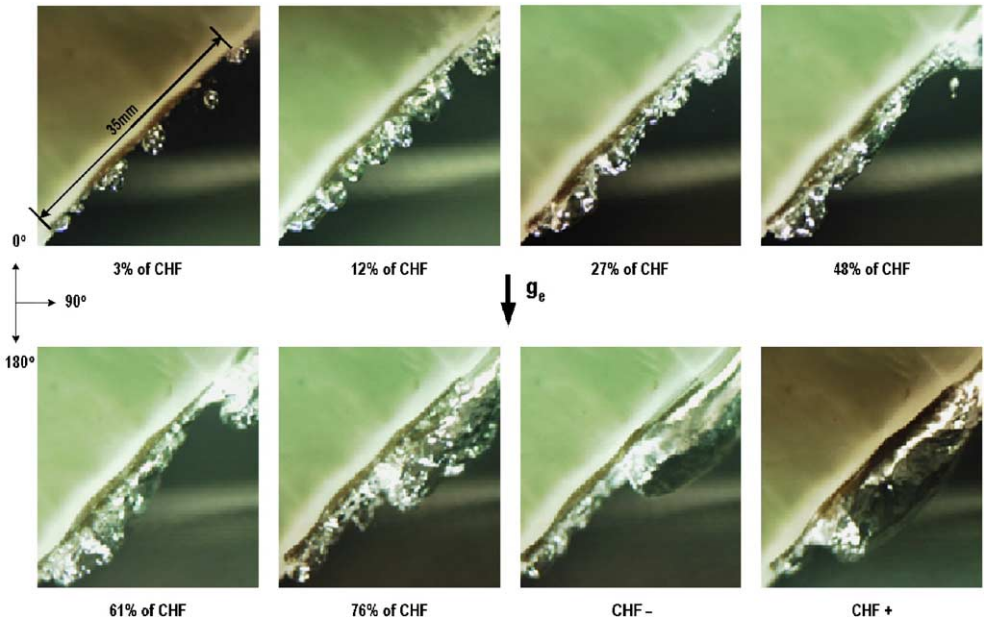

Fig. 8. Flow visualization (open periphery, 135°).

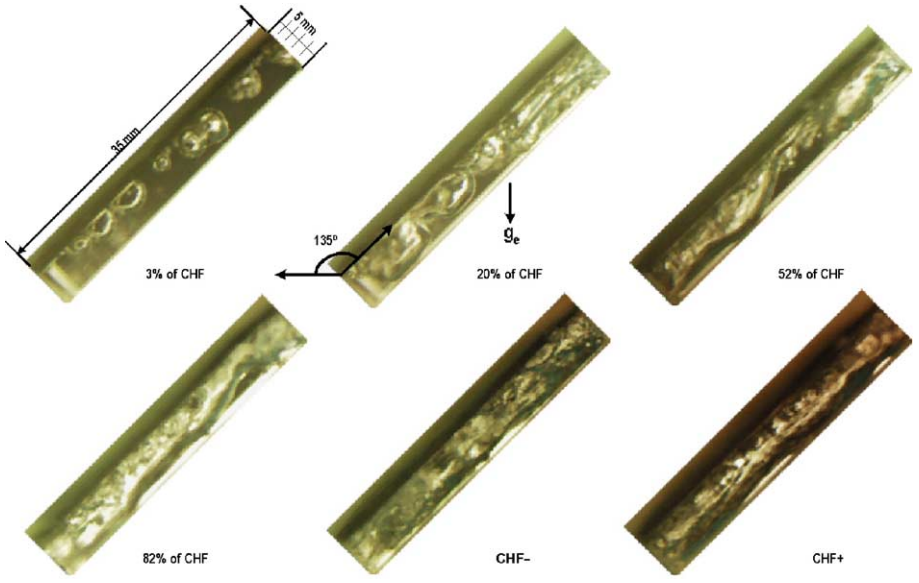

Fig. 9. Flow visualization (5 mm, 135°).

the open periphery. The heat transfer coefficient in the vicinity of CHF in the open periphery at 95° inclination, for instance, is less than that in the 5 mm gap. Conversely, the CHF at such location is larger than that in the 5 mm gap. This may be attributed to the fact that the gap structure

can give rise to the higher mass flux compared with that in the open periphery. The gap structure can restrict the vapor growth toward the normal direction to the surface from which heat is removed. This in turn redirects the vapor flow to become more parallel to the surface. Accordingly, the mass flux by restricting the gap structure can increase, and thus the higher mass flux can induce the higher heat transfer coefficient.

3.2. Pool and gap boiling visualization in vertical region

Fig. 10 illustrates the fundamental pool boiling characteristics photographed by the side and front of the test heater in the vertical location (90°). Figs. 11–13 present the bubble growth and coalescence in the 2, 5 and 10 mm gaps at the same location, respectively.

There may be the mirage effect in the visualization results (Cooper, 1983; Mayinger, 1995). As depicted in Figs. 10 and 11, the photos taken in the front show that the bubbles cover the entire heater surface prior to the CHF point (about 60% CHF), falsifying that the CHF has already been approached. The amount of deflection depends on how much of the optical path to the camera lies within the region of high temperature gradient, which is maximized for a plane wall, in case of this experiment. This requires careful assessment of the bubbles viewed in profile on the boundary of a cylinder and sphere (Kenning, 2004). Despite the maximum mirage effect in the plane wall as tested in this experiment, these photos in the side advocate that the mirage effect has a minimal influence. Deflection and chromatic aberration, the controlling factors of the mirage effect, were reduced by the polarization and achromatic lenses attached in the camera. When the temperature of water on the heating surface approached the CHF point, the differences in water density did not produce the significant refraction due to rapid wakes (i.e. the breakdown and exchange of the thermal boundaries of water on the heating surface).

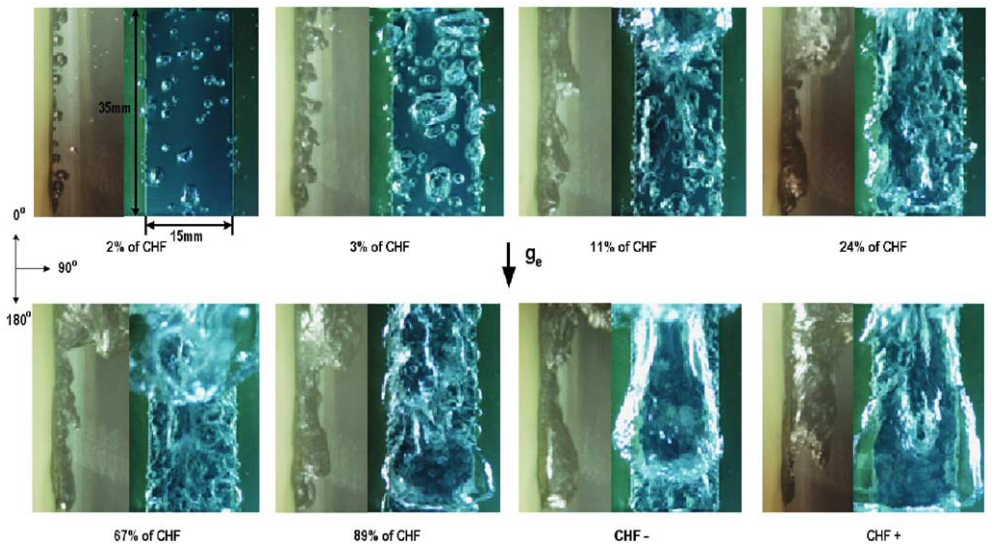

Fig. 10. Flow visualization (open periphery, 90°).

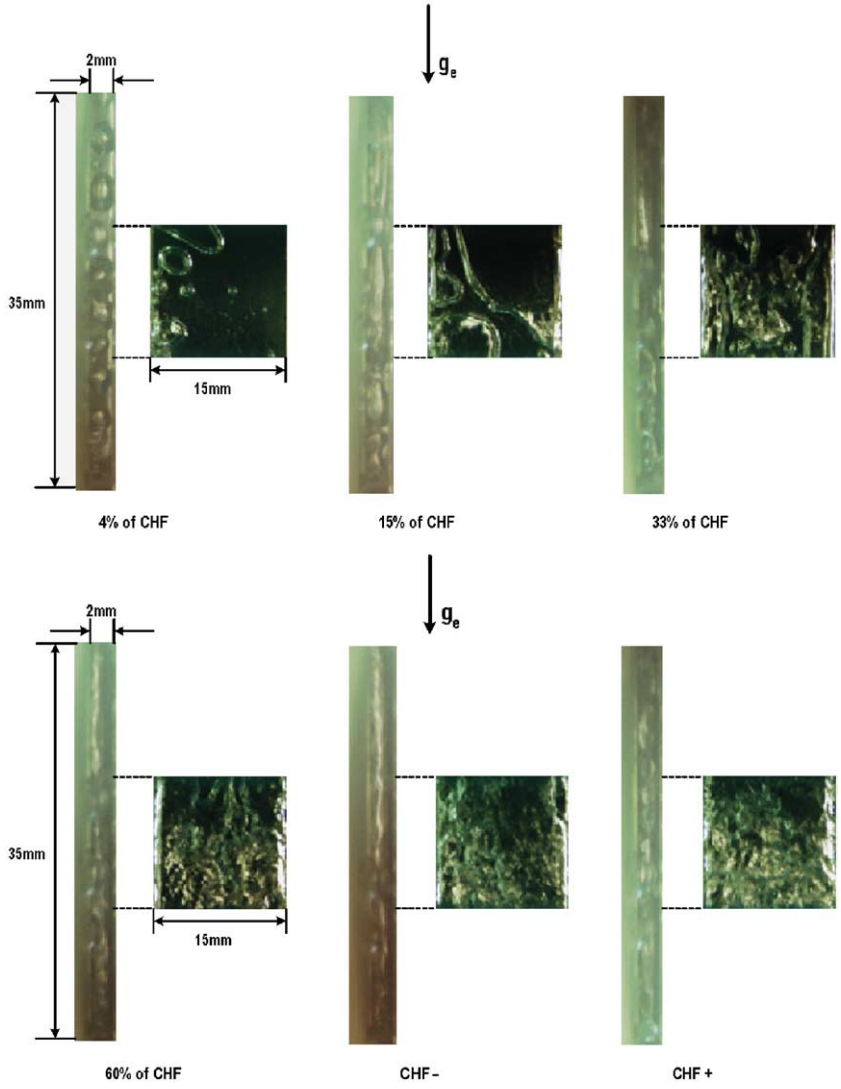

Fig. 11. Flow visualization (2 mm, 90°).

In analyzing these two kinds of boiling states, the vapor behavior confined by the gap structure is more vigorous than in the open periphery, in which the complexity of the flow mode may be due to the convective force resulting from the gap structure. However, inherently larger CHF in pool boiling than gap boiling will hold because the bubbles can escape from the channel more easily. Note in Fig. 10 that the vapor motion right before the CHF, say, CHF−, exhibits a typical pattern of the Helmholtz wavy motion. The convex vapor shape at the bottom of the vapor streak suggests a higher vapor pressure. Conversely, the concave shape at the top of vapor streak indicates the lower vapor pressure than the liquid pressure, which may explain the inertial limited bubble growth in the vicinity of liquid. This limitation is determined by how rapidly it can push back the

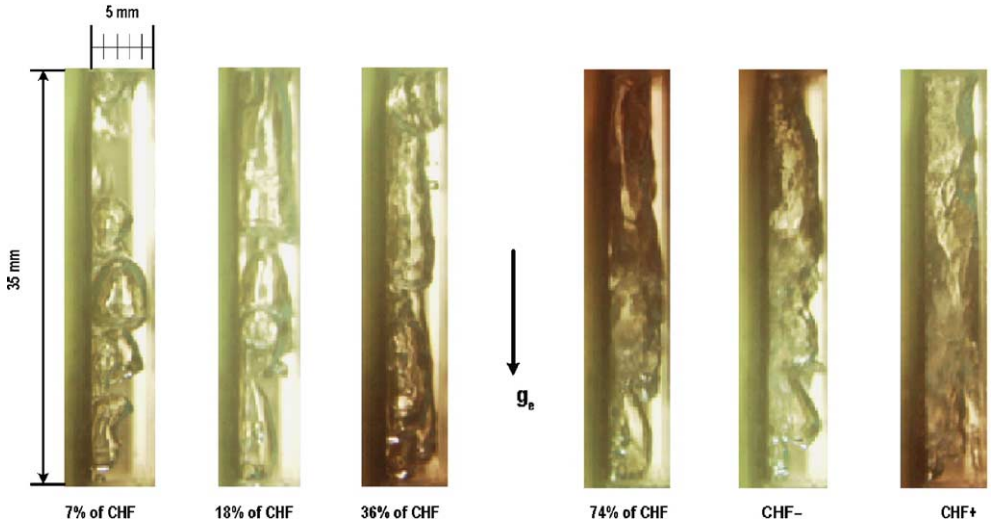

Fig. 12. Flow visualization (5 mm, 90°).

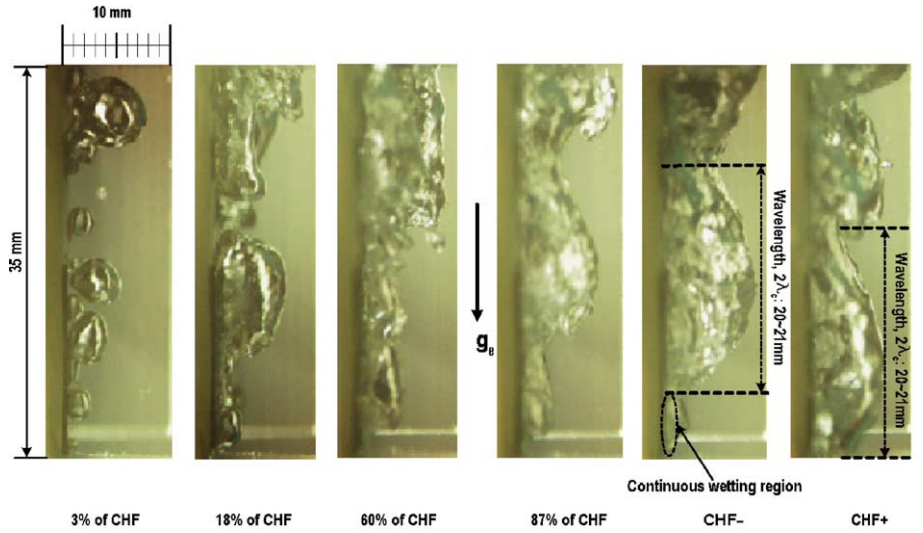

Fig. 13. Flow visualization (10 mm, 90°).

surrounding liquid, which may give an essential clue to determining the critical wavelength. This is important in predicting the heat transfer rate. The reason is that the critical Helmholtz velocity can be calculated once the critical wavelength is found experimentally and theoretically. Accordingly, this information can be utilized to determine the mass flow rate of the vapor phase.

Figs. 11–13 depict the typical gap boiling phenomena in the vertical channel, in which inherently larger bubbles compared with those of the refrigerant and cryogenic fluid (Carey, 1992) play an important role in triggering the CHF. In Fig. 11 the vapor generation states are photographed

as the heat flux increases. From the initial stage of boiling, bubbles are dispersed and coalesced due to the narrow gap. As the heat flux increases, more vigorous vapor motions are observed and the liquid deficient fronts diminish. In the vicinity of the CHF, the vapor layer coalesced and dispersed by the individual vapor covering most regions of the channel, which induces relatively low CHF in the 2 mm gap compared with that in the open periphery. In case of visualization in the 10 mm gap, the average vapor layer thickness is larger than the gap size of 5 mm (about 6 mm), and hence, the seeming Helmholtz wavy motion in the 10 mm gap is disturbed in the 2 and 5 mm gap boiling. The CHF increases as the gap size increases mainly due to the dominant buoyant force.

3.3. Gap boiling visualization in downward-facing region

In the completely downward-facing region (180°), the bubble movements may be significantly restricted by the geometry. In this sense, the photograph of such situations in this region provides insights to well predict the CHF as well as the nucleate boiling regime. In order to enhance the predictive capability of the CHF including general two-phase flow analysis, rigorous study in the confined channel was carried out resorting on the visualization results.

Figs. 14 and 15 visualize the two-phase flow in the completely downward-facing location (180°), in which the gap sizes are 5 and 10 mm, respectively. In Fig. 14, the bubbles in the gap are squeezed and dispersed in the vicinity of the CHF by the gap structure, and hence those tend to be ejected due to the induced flow effect. In Fig. 15, on the other hand, the vapor layer thickness in the 10 mm gap is about 6–7 mm, which is smaller than the gap size of 10 mm. For the characteristic of completely downward-facing location (180°), the buoyant force is hampered significantly. Instead, the behavior is primarily affected by the momentum of the vapor rising from the wetted front. Thus the vapor appears to be stagnated without escaping, which causes a lower CHF than in the 5 mm gap. This result repeats itself in the 1 and 2 mm gaps. Table 1 presents the values of CHF for different surface orientation angles and gap sizes. In vertical regions (90°), the

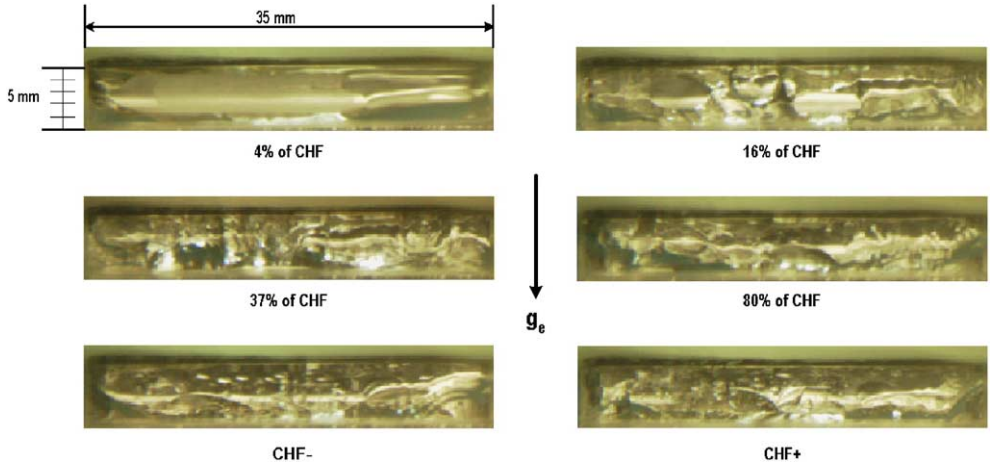

Fig. 14. Flow visualization (5 mm, 180°).

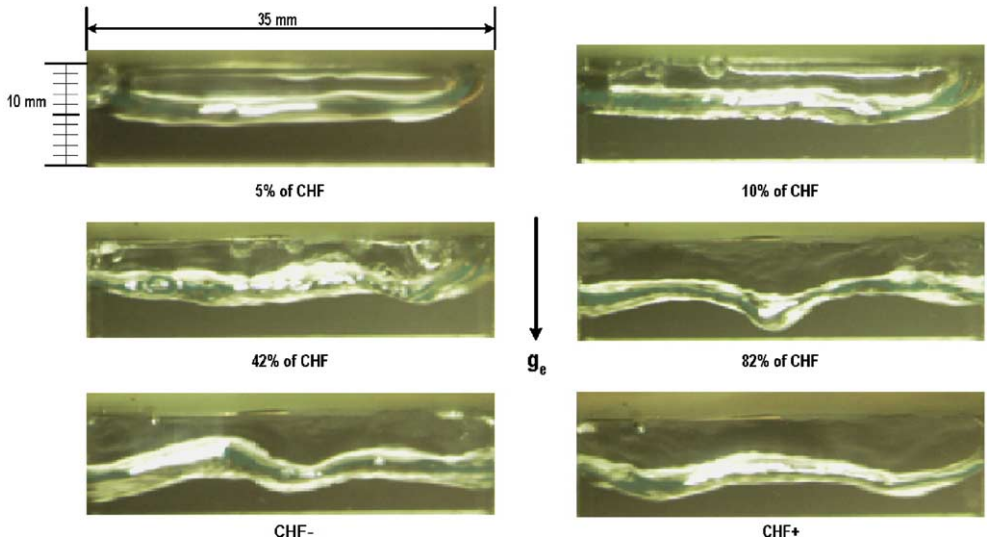

Fig. 15. Flow visualization (10 mm, 180°).

Table 1
CHF for gap size and surface orientation angle (kW/m^2)

Gap size (mm)	Angle											
	90°	95°	105°	115°	125°	135°	145°	155°	165°	170°	175°	180°
1	598.4	585.2	570.6	556.1	542.0	480.9	435.6	374.8	359.5	351.4	317.9	296.7
2	984.6	969.4	954.3	937.2	900.5	860.3	803.3	702.6	526.5	448.2	369.8	282.0
5	1197	1178	1164	1151	1105	1088	1049	972.3	876.9	793.5	646.7	228.7
10	1204	1189	1153	1120	1062	1025	976.7	918.4	848.7	793.1	751.1	167.1
Pool	1341	1320	1310	1244	1276	1189	1110	1128	1128	1108	1068	962.4

CHF increased as the gap size increased consistent with findings from several previous studies. In downward-facing region (180°), however, the opposing results were observed, i.e. the CHF increased as the gap size decreased.

3.4. Gap size and surface orientation effect

In Fig. 16, several two-phase flow photographs in the vicinity of the CHF are presented in terms of the surface orientation angle in the 5 and 10 mm gaps. The snapshots help explain the combined effect of gap size and gravity in the rectangular channel.

Visual inspection of the fluid motion in the rectangular channel captured in Fig. 16 revealed that the Helmholtz instability was not observed in the 1 and 2 mm gaps. In most surface inclinations of 5 mm gap boiling, similar dispersed and coalesced vapor motion by the gap structure was detected excluding at certain inclination angles that may be interpreted as the Helmholtz instability motion. In the 10 mm gap boiling, however, the Helmholtz instability motion exists over the broad surface inclination angle. In particular, a wavelength of about 21 mm was observed at the

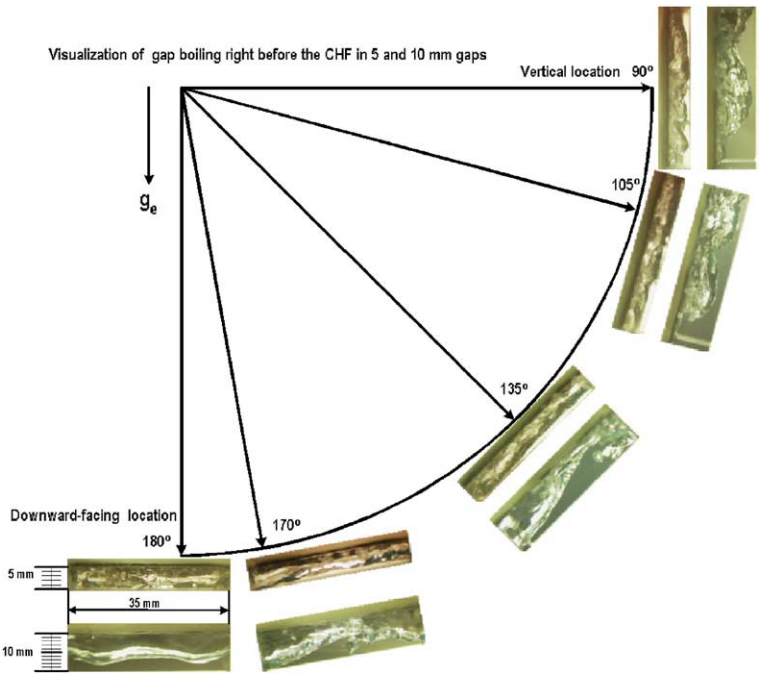

Fig. 16. Flow visualization at CHF– concerning surface orientation (5 and 10 mm).

vertical position (90°) in the 10 mm gap. Except for the angle of 180°, most of the vapor motions in the 10 mm gap have the characteristic of the Helmholtz instability near CHF, and this is typified in the vertical location. In the 5 mm gap boiling, however, the vapor movements are dominantly induced by the gap in the completely downward-facing location (180°). This induced flow effect is weakened as the surface inclination approaches the vertical location (90°), in which buoyancy mainly affects the two-phase flow and accordingly the CHF.

Fig. 17 represents the CHF data varying with the gap size and surface inclination angle. Fig. 18 also shows the CHF data for pool boiling with open periphery.

Until now it has generally been claimed that the CHF decreases as the gap size decreases. Contrary to this general belief, however, the present study has found opposing results at certain surface inclination angles. At the vertical location (90°), in consistency with the general belief, the CHF decreases as the gap size decreases. Especially, the CHF for the gap size of 10 mm is smaller than that for any other gap sizes at the fully downward-facing location (180°) as shown in Figs. 17 and 18 and Table 1.

More detailed explanations shall shed light on understanding of the current finding that the CHF generally increases as the gap size increases, but the increasing rate decreases with an exception at the fully downward-facing angle as depicted in Fig. 17. The experimental data in this study are compared with other results reported in the literature. In the vertical rectangular geometry of Monde et al. (1982) and Xia et al. (1996), the increasing trend of the CHF with the gap size is compared with the present experimental data. It is found that the CHF changing trend differs with geometry. Though the overall behavior of CHF in the horizontal co-axial disk is comparable, the

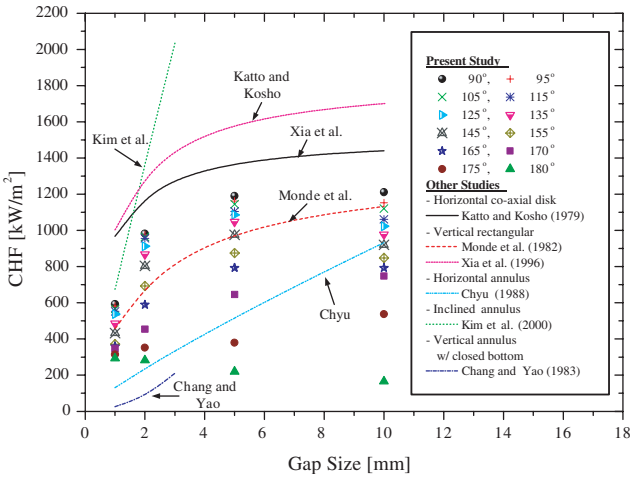

Fig. 17. Effect of gap size on CHF.

CHF is grossly overpredicted. Monde et al.'s correlation appears to reasonably represent the current experimental data. Accounting for the gravity effect in Eq. (3), Monde et al.'s correlation is compared with the CHF in the gap and pool boiling as shown in Fig. 18(a). While underestimating CHF for the 1, 2 and 5 mm gaps, their correlation satisfactorily predicts CHF for the 10 mm gap and pool boiling for most of the angles below, say, 150°.

Fig. 18(a) and (b) demonstrate that the CHF for 1 and 2 mm gaps decreases as the inclination angle increases and as the gap size decreases except at the fully downward-facing location (180°). As mentioned earlier, at the downward-facing angle, the bubble formed in the gap smaller than its thickness is affected by the induced flow effect due to the gap. In other words, bubbles in the narrow gap can more easily escape from the restricted channel than those in the gap whose size exceeds the bubble thickness. Though the bubble in the 1, 2 and 5 mm gaps tends to be ejected due to the induced flow effect, the bubble in the 10 mm gap is stagnated. That is, the induced flow effect increases as the gap size decreases at the fully downward-facing angle. Hence, at that location, the CHF decreases as the gap size increases contrary to the trend at other angles. However, the CHF in the pool boiling with the open periphery is greater than that in the gap boiling because the bubble in the pool boiling with open periphery is free to escape in the azimuthal direction.

While the CHF values for the 5 and 10 mm gaps both decrease as the inclination angle increases, the CHF for the 10 mm gap is less than that for the 5 mm gap over a wide range of angles due to absence of the induced flow effect in the 10 mm gap as portrayed in Fig. 18(b). The flow rate depends on the balance between the driving force and the pressure drop. The driving force for the 5 mm gap is larger than that for the 10 mm gap size due to high void fraction within the confined channel space. Given the flow rate, the pressure drop for the 5 mm gap is greater than that for the 10 mm gap. Then, the mass flux for the 5 mm gap can exceed that for the 10 mm gap due to the smaller flow area over a span of the inclination angles. Consequently, there can be a range of inclination angles over which the CHF increases as the gap size decreases. Interestingly enough, this newly theorized thermal hydraulic phenomenon appears to unmistakably take place at the fully downward-facing angle for all the gap sizes examined in this work, and occasionally

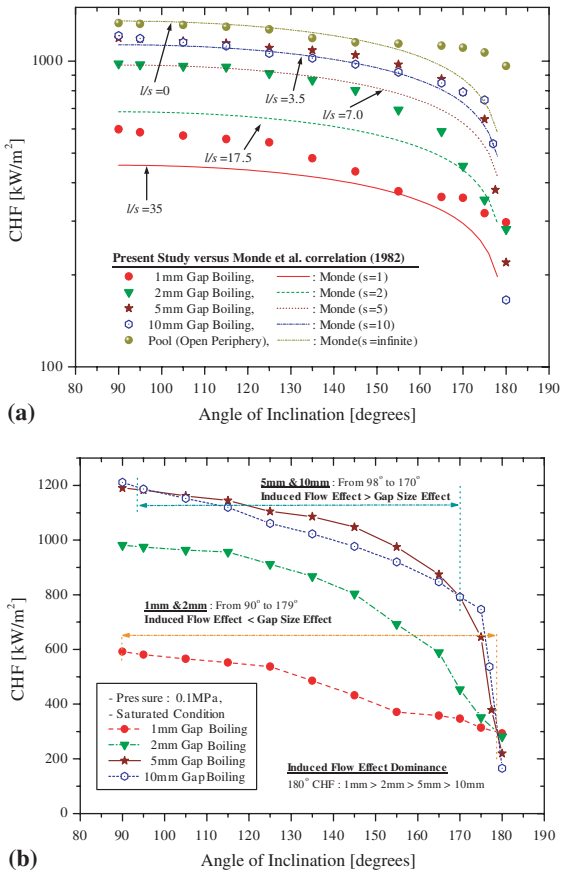

Fig. 18. Effect of surface inclination angle on CHF. (a) Comparison against the Monde et al. correlation. (b) Effect of induced flow and gap size on CHF.

over some range of angles for the 5 and 10 mm gaps. Therefore, the CHF in the gap boiling is affected by the gap size as well as by the induced flow within the gap.

3.5. Interfacial instability of vapor layer

Mudawar et al. (1997) predicted and solved for the interfacial instability of vapor layer in vertical pool boiling by photographing the vapor layer for water as well as for FC-72 under the atmospheric pressure. They suggested the separated flow model and solved it analytically for some limiting cases, in which the average vapor velocity and critical wavelength were obtained. In present study, a similar instability behavior at 10 mm gap boiling was observed as presented in Fig. 13. Relatively short heater length compared with several cycles of wavelength calculated from the classical instability theory, however, makes it hard to precisely determine its repeatability directly from photograph. Although the repeated cycle of the instability behavior was not exactly discernable, wetting front propagation along a vertical surface can be predicted based upon the present photographic study and previous study of Mudawar et al. (1997). Fig. 19 shows the schematic

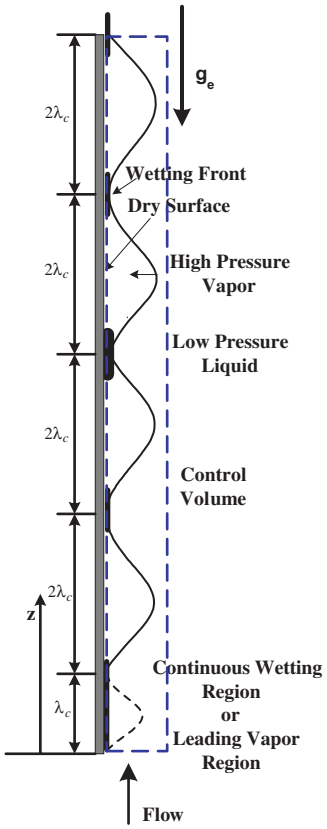

Fig. 19. Schematic diagram of interfacial instability.

diagram of the interfacial instability, where the leading edge at the bottom of the test heater is repeatedly wetted by the vapor generation. Departed from the continuous wetting region in the leading edge, the wetting fronts are formed when a disturbance in the liquid–vapor interface becomes unstable during the growing of its amplitude until the interface contacts with the heater surface. Until reaching the CHF, wetting fronts keep in contact with the heater surface. In the vicinity of the CHF, however, the momentum of the vapor generation overcomes the pressure force exerted on the liquid–vapor interface and thus the CHF triggers. The pressure force plays an important role in perturbing the interfacial stability, while the momentum of the vapor generation tends to lift the wetting fronts off. The instability primarily occurs when the velocities of liquid and vapor are different. In the region of vertical pool boiling, the liquid–vapor velocity has difference in identity, in which the gravitational force may be weakened. With the aid of simple classical instability theory and the study of Mudawar et al. (1997), the critical wavelength in the 10 mm vertical gap boiling that is similar to vertical pool boiling as well as flow boiling, λ_c, was calculated based on the present experimental CHF data.

Mudawar et al. (1997) proposed a lift-off criterion as the CHF trigger mechanism, in which they assured that the CHF would occur when the upstream wetting front lifts off the heater surface. They reported that this occurs when the localized heat flux at the wetting front is large enough

that the normal momentum of vapor generated in the wetting front just exceeds the pressure force exerted upon the interface as a result of the interfacial curvature. The pressure difference resulting from a sinusoidal disturbance of the form perpendicular to the unperturbed interface can be expressed as

$$\begin{aligned} &P_{\mathrm{L}} - P_{\mathrm{G}} = -\eta k[\rho''_{\mathrm{L}}(c-\bar{u}_{\mathrm{L}})^2 + \rho''_{\mathrm{G}}(c-\bar{u}_{\mathrm{G}})^2] - (\rho_{\mathrm{L}}-\rho_{\mathrm{G}})g_n\eta = -\sigma k^2\eta \\ &\eta(z,t) = \eta_0 \mathrm{e}^{\mathrm{i}k(z-ct)} \\ &\rho''_{\mathrm{L}} = \rho_{\mathrm{L}}\coth(kh_{\mathrm{L}}) \\ &\rho''_{\mathrm{G}} = \rho_{\mathrm{G}}\coth(kh_{\mathrm{G}}) \end{aligned} \tag{4}$$

where P_{L} and P_{G} are the liquid and vapor pressure exerted on the interfacial curvature, η is the interfacial displacement, η_0 is the amplitude of interfacial displacement, k is the wave number, c is the wave speed, $\bar{u}_{\mathrm{L}}$ and $\bar{u}_{\mathrm{G}}$ are the mean velocity of liquid and vapor, g_n is the body force per unit mass perpendicular to the unperturbed interface, ρ''_{L} and ρ''_{G} are the modified density terms of liquid and vapor for a straight heater, h_{L} and h_{G} are the mean liquid and vapor layer thickness, respectively. Solving Eq. (4) for the wave speed, c, and utilizing the fact that for vertical pool boiling, $g_n = 0$, $\bar{u}_{\mathrm{L}} = 0$, $\rho''_{\mathrm{L}} = \rho_{\mathrm{L}}$, and $\rho''_{\mathrm{G}} \approx \rho_{\mathrm{G}}$, the following equation results

$$c = \frac{\rho_{\mathrm{G}}\bar{u}_{\mathrm{G}}}{(\rho_{\mathrm{G}}+\rho_{\mathrm{L}})} \pm \sqrt{\frac{\sigma k}{(\rho_{\mathrm{G}}+\rho_{\mathrm{L}})} - \frac{\rho_{\mathrm{G}}\rho_{\mathrm{L}}\bar{u}_{\mathrm{G}}^2}{(\rho_{\mathrm{G}}+\rho_{\mathrm{L}})^2}} \tag{5}$$

When the liquid–vapor interface becomes unstable, the wave speed can be expressed as an imaginary number, with a real component

$$c_{\mathrm{r}} = \frac{\rho_{\mathrm{G}}\bar{u}_{\mathrm{G}}}{(\rho_{\mathrm{G}}+\rho_{\mathrm{L}})} \tag{6}$$

and an imaginary component

$$c_{\mathrm{i}} = \sqrt{\frac{\rho_{\mathrm{G}}\rho_{\mathrm{L}}\bar{u}_{\mathrm{G}}^2}{(\rho_{\mathrm{G}}+\rho_{\mathrm{L}})^2} - \frac{\sigma k}{(\rho_{\mathrm{G}}+\rho_{\mathrm{L}})}} \tag{7}$$

The critical wavelength, or the wavelength that produces a stable wave, can be calculated by setting c_{i} in Eq. (7) equal to zero, such that

$$\lambda_{\mathrm{c}} = \frac{2\pi}{k_{\mathrm{c}}} = \frac{2\pi\sigma(\rho_{\mathrm{L}}-\rho_{\mathrm{G}})}{\rho_{\mathrm{L}}\rho_{\mathrm{G}}\bar{u}_{\mathrm{G}}^2} \tag{8}$$

where λ_{c} is the critical wavelength and k_{c} is the critical wave number.

In addition, integrating with respect to z after combining the mass and energy conservations for the streamwise vapor layer length $\mathrm{d}z$ yields

$$\rho_{\mathrm{G}}\bar{u}_{\mathrm{G}}\delta = \frac{q_{\mathrm{CHF}}z}{h_{\mathrm{LG}}\left(1+\frac{c_{p,\mathrm{L}}\Delta T_{\mathrm{sub}}}{h_{\mathrm{LG}}}\right)} \tag{9}$$

where δ is the vapor layer thickness, h_{LG} is the latent heat of vaporization, $c_{p,\mathrm{L}}$ is the specific heat of water and ΔT_{sub} is the liquid subcooling.

On the same control volume, momentum balance under the assumption of a stationary process yields

$$\frac{\mathrm{d}}{\mathrm{d}z}(\rho_{\mathrm{G}}\bar{u}_{\mathrm{G}}^2\delta) = (\rho_{\mathrm{L}} - \rho_{\mathrm{G}})g\delta - \tau_{\mathrm{i}} - \tau_{\mathrm{w}}\left(1 + \frac{2\delta}{w}\right) \tag{10}$$

where the interfacial and wall shear stress, τ_{i} and τ_{w}, respectively, are defined as

$$\tau_{\mathrm{i}} = 0.5 f_{\mathrm{i}}\rho_{\mathrm{G}}\bar{u}_{\mathrm{G}}^2 \tag{11}$$

$$\tau_{\mathrm{w}} = 0.5 f_{\mathrm{w}}\rho_{\mathrm{G}}\bar{u}_{\mathrm{G}}^2 \tag{12}$$

In Eq. (11), the interfacial friction factor, f_{i}, was assumed to have a constant value of 0.5, as proposed by Galloway and Mudawar (1993), and Gersey and Mudawar (1995). They suggested that this value provided the best agreement between measured and predicted pressure drops obtained from flow boiling studies. Further, their parametric study of the interfacial friction factor values for vertical pool boiling indicates that the interfacial friction factor ranging from 0.25 to 1.0 does not significantly affect the separated flow model. In Eq. (12), the wall friction factor, $f_{\mathrm{w}} = 0.0791/Re^{0.25}$, was set from the Blasius correlation for turbulent flow, in which the Reynolds number is based on the hydraulic diameter of the vapor layer, say, $2w\delta/(w+\delta)$, in which w denotes the heater width.

Combining of Eq. (9) with Eq. (11) yields a differential equation for vapor velocity $\bar{u}_{\mathrm{G}}$ and axial location z. For some limiting cases, the wall shear stress and momentum gradient in Eq. (10) are neglected, and $\bar{u}_{\mathrm{G}}$ would be approximately

$$\bar{u}_{\mathrm{G}} = \left\{ \left(\frac{\rho_{\mathrm{L}} - \rho_{\mathrm{G}}}{\rho_{\mathrm{G}}}\right) \frac{q_{\mathrm{CHF}}}{0.5 f_{\mathrm{i}}\rho_{\mathrm{G}} h_{\mathrm{LG}}\left(1 + \frac{c_{p,\mathrm{L}}\Delta T_{\mathrm{sub}}}{h_{\mathrm{LG}}}\right)} gz \right\}^{1/3} \tag{13}$$

In Fig. 19, the first wetting front is referenced at $z = \lambda_{\mathrm{c}}$, presumably. Hence substituting Eq. (8) into Eq. (13) with respect to the vapor velocity $\bar{u}_{\mathrm{G}}$ for the $z = \lambda_{\mathrm{c}}$ yields

$$\lambda_{\mathrm{c}} = \left(\frac{2\pi\sigma(\rho_{\mathrm{L}} + \rho_{\mathrm{G}})}{\rho_{\mathrm{L}}\rho_{\mathrm{G}}}\right)^{3/5} \cdot \left\{ \left(\frac{\rho_{\mathrm{L}} - \rho_{\mathrm{G}}}{\rho_{\mathrm{L}}\rho_{\mathrm{G}}}\right) g \cdot \frac{q_{\mathrm{CHF}}}{0.5 f_{\mathrm{i}}\rho_{\mathrm{G}} h_{\mathrm{LG}}\left(1 + \frac{c_{p,\mathrm{L}}\Delta T_{\mathrm{sub}}}{h_{\mathrm{LG}}}\right)} \right\}^{-2/5} \tag{14}$$

where g represents the gravitational acceleration.

In the present study, experiments are conducted for saturated water at the atmospheric pressure. Thus, the liquid subcooling in Eq. (14), ΔT_{sub}, should be arranged to be zero. In addition, the maximum heat flux can be replaced with the present experimental CHF data in the 10 mm gap boiling in vertical region (90°). Then final form of the critical wavelength equation is given by

$$\lambda_{\mathrm{c}} = \left(\frac{2\pi\sigma(\rho_{\mathrm{L}} + \rho_{\mathrm{G}})}{\rho_{\mathrm{L}}\rho_{\mathrm{G}}}\right)^{3/5} \left(\frac{(\rho_{\mathrm{L}} - \rho_{\mathrm{G}})}{\rho_{\mathrm{L}}\rho_{\mathrm{G}}} g \cdot \frac{q_{\mathrm{CHF}}}{0.5 f_{\mathrm{i}}\rho_{\mathrm{G}} h_{\mathrm{LG}}}\right)^{-2/5} \tag{15}$$

The CHF in the 10 mm gap boiling at vertical location (90°) was 1.204×10^6 W/m^2 and the corresponding critical wavelength calculated by Eq. (15) is 9.5 mm. Hence $2\lambda_c = 19$ mm. This is approximately close to that shown in Fig. 13.

3.6. Transition angle

In recent years, some researchers have mentioned the existence of a transition angle at which the CHF changes with a rapid slope. Howard and Mudawar (1999) suggested that based on the vapor behavior observed just prior to the CHF, the surface orientations can be divided into three regions: upward-facing (0°–60°), near-vertical (60°–165°) and downward-facing (>165°). Yang et al. (1997) noticed that a transition angle exists in the boiling behavior from vertical-like to downward-facing between 150° and 174°. The transition angle is defined as the boundary between the near-vertical and downward-facing regions.

In the present study, certain transition angles were also identified for different gap sizes. For the gap size of 1 mm and pool boiling with an open periphery, the existence of the transition angle was not discernable as shown in Fig. 20(a) and (b). However, in the experiments for the gap sizes of 2, 5 and 10 mm, the transition angles were observed as shown in Fig. 20(a). For the gap sizes of 2, 5 and 10 mm, the transition angles were found to be 165°, 170° and 175°, respectively. At heat fluxes approaching the CHF, the boiling process can be divided into two regions with categorically different slopes in terms of the non-dimensionalized CHF. The near-vertical region is defined as the angular range from vertical (90°) to transition, while the downward-facing region is defined as the angular span from transition to completely downward-facing (180°). Albeit Howard and Mudawar (1999) and Yang et al. (1997) claimed a transition angle for the pool boiling CHF with open periphery, the current investigation could not necessarily confirm their claims. The reason may well be that the aspect ratio of the heater width to length in this study is considerably smaller than that in their experiments. Specifically, the heater aspect ratio is 2.3 in this study versus 10.9 and about 10 in Howard and Mudawar (1999) and Yang et al. (1997), respectively. It was also found that the values of $q_{CHF}/q_{CHF,90}$ for differing gap sizes are more broadened as the surface inclination angle increases as shown in Fig. 20(a) and (b).

The non-dimensionalized CHF data in this work are compared with predictions by literature correlations developed from tests utilizing such varying fluids as FC-72, water, R113 and liquid-helium in Fig. 20(b). The non-dimensionalized form of the correlations in the cited literature is seen to shift for differing fluids, which appears to support El-Genk and Guo's (1993) assertion that different correlations be used for different fluids in describing the effect of orientation on the CHF. Howard and Mudawar (1999) confirmed different transition angles for different fluids, viz. 150° for liquid helium, and 160° to 165° for water and FC-72. Fig. 20(b) demonstrates that one non-dimensionalized equation cannot possibly correlate the experimental data at various inclination angles, because the non-dimensionalized CHF values tend to spread with increasing angles beyond the acceptable error range. That is, the non-dimensionalized correlation will be affected not only by different fluid properties, but also by the surface orientation effect. It is also noted that the Monde et al. (1982) and Chang and You (1996) correlations provide respectively with the upper and lower bounds for the data taken from the present study.

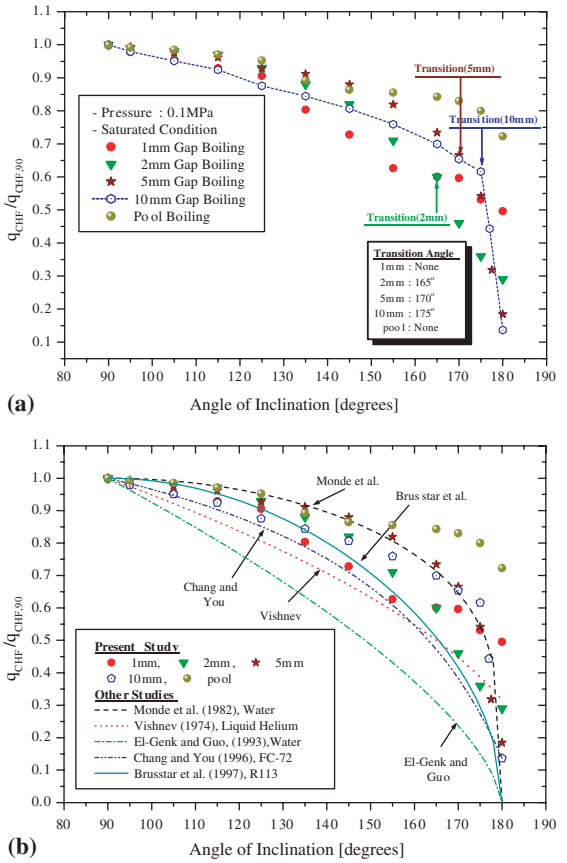

Fig. 20. Effect of surface inclination angle on CHF. (a) Transition angles for differing gaps. (b) Comparison of angle effect.

4. Conclusions

In the present study, the CHF experiments were carried out for narrow gaps of 1, 2, 5 and 10 mm, in which the surface orientation effect was taken into account by varying the rectangular heater assembly having a heater length of 35 mm from vertical location (90°) to downward-facing location (180°) for distilled water under the atmospheric pressure. In addition, the experiment for pool boiling with the open periphery was performed. While the quantitative CHF data were obtained by monitoring the temperature profile during experiments, in each stage of heat flux increase the two-phase flow movements were also photographed by using the high-speed digital camera. Major conclusions from the present study may be summarized as follows:

- The visualization study both for the gap and pool boiling phenomena was conducted by using the high-speed camera devices. The pool and gap boiling in the inclined downward and upward-facing regions, 45° and 135°, was addressed in terms of the gravitational and buoyant forces. The pool and gap boiling in the vertical region, 90°, was photographed approaching the

CHF, in which the buoyant force dominates over all the other forces. The gap boiling characteristics were presented, in which the infeasibility of vapor escape gives rise to the lower CHF as the gap size increases.

- The gap size and surface orientation effects play a crucial role in interpreting the general two-phase flow behavior as well as the CHF data. There exists a critical gap size commensurate to the average vapor layer thickness enhancing the heat transfer rate with increasing mass flux at a certain surface orientation. Associated with the photographing study, the quantitative CHF data were obtained. It was observed that the CHF generally increases as the gap size increases, but the increasing rate decreases as the gap increases. At the vertical location (90°), as is generally believed, the CHF increases as the gap size increases. However, the CHF in the gap size of 10 mm is smaller than the value at any other gap sizes at the fully downward-facing location (180°). The CHF in gap boiling is affected by the gap size as well as by the induced flow within the channel.
- The competing forces of the pressure force exerted on the liquid–vapor interface and the momentum of vapor generation tends to keep the sinusoidal wave. In the present experimental study, the interfacial instability of the vapor layer was detected in the 10 mm gap boiling, in which the critical wavelength, $\lambda_c = 10$–10.5 mm was compared with the result of analytic equation solved based upon the classical hydrodynamic instability theory for some limiting cases. The calculated critical wavelength was 9.5 mm close to the detected critical wavelength in the vertical 10 mm gap boiling.
- There is a transition angle for each gap size. The transition angle increase as the gap size increases. The transition angles for the 2, 5 and 10 mm gap sizes were distinctly found to be 165°, 170° and 175°, respectively. However, existence of a transition angle was not discernable for the gap size of 1 mm and the pool boiling in the unconfined space. The non-dimensional $q_{CHF}/q_{CHF,90}$ values for each gap size at the same angle show greater spread in the data as the surface inclination angle increases.

Acknowledgements

This work was performed under the auspices of the Korean Ministry of Science and Technology (contract number M20112000001-01B0300-00210) and US Department of Energy (contract number DE-ACO7-991D13727) as an International Nuclear Energy Research Initiative project awarded to the Seoul National University and the Idaho National Engineering and Environmental Laboratory in collaboration with the Korea Atomic Energy Research Institute and the Pennsylvania State University.

References

Brusstar, M.J., Merte, H., 1994. Effects of buoyancy on the critical heat flux in forced convection. J. Thermophys. Heat Transf. 8, 322–328.

Brusstar, M.J., Merte, H., Keller, R.B., Kirby, B.J., 1997. Effects of heater surface orientation on the critical heat flux—I. An experimental evaluation of models for subcooled pool boiling. Int. J. Heat Mass Transf. 40, 4007–4019.

Carey, V.P., 1992. Liquid–Vapor Phase-Change Phenomena: An Introduction to the Thermophysics of Vaporization and Condensation Processes in Heat Transfer Equipment. Hemisphere Publishing Corporation, New York, NY, USA.

Chang, J.Y., You, S.M., 1996. Heater orientation effects on pool boiling of micro-porous-enhanced surfaces in saturated FC-72. Trans. ASME, J. Heat Transf. 118, 937–943.

Chang, Y., Yao, S., 1983. Critical heat flux of narrow vertical annuli with closed bottoms. ASME J. Heat Transf. 105, 192–195.

Cheung, F.B., Yang, J., Dizon, M.B., Rempe, J.L., Suh, K.Y., Kim, S.B., 2004. Scaling of downward facing boiling and steam venting in a heated hemispherical annular channel. Int. J. Transport Phenom. 6, 81–96.

Cho, J.S., Suh, K.Y., Chung, C.H., Park, R.J., Kim, S.B., 2000. The effect of coolant boiling on the molten metal pool heat transfer with local solidification. J. Korean Nucl. Soc. 32, 34–45.

Cho, J.S., Suh, K.Y., Chung, C.H., Park, R.J., Kim, S.B., 2004. Enhanced natural convection in metal layer cooled by boiling water. Nucl. Tech. 148, 313–324.

Chyu, M.C., 1988. Prediction of boiling dryout flux for restricted annular crevice. Int. J. Heat Mass Transf. 31, 1993–1998.

Cooper, M.G., 1983. The mirage in boiling. Int. J. Heat Mass Transf. 26, 1088–1090.

Dizon, M.B., Yang, J., Cheung, F.B., Rempe, J.L., Suh, K.Y., Kim, S.B., 2004. Effects of surface coating on the critical heat flux for pool boiling from a downward facing surface. J. Enhanced Heat Transf. 11, 133–150.

El-Genk, M.S., Guo, Z., 1993. Transient boiling from inclined and downward-facing surfaces in a saturated pool. Int. J. Refrigeration 6, 424–432.

Galloway, J.E., Mudawar, I., 1993. CHF mechanism in flow boiling from a short heated wall—II. Theoretical CHF model. Int. J. Heat Mass Transf. 36, 2527–2540.

Gersey, C.O., Mudawar, I., 1995. Effects of heater length and orientation on the trigger mechanism for flow boiling CHF—II. CHF model. Int. J. Heat Mass Transf. 38, 643–654.

Githinji, P.M., Sabersky, R.H., 1963. Some effects of the orientation of the heating surface in nucleate boiling. Trans. ASME, J. Heat Transf. 85, 379.

Guo, Z., El-Genk, M.S., 1992. An experimental study of saturated pool boiling from downward facing and inclined surfaces. Int. J. Heat Mass Transf. 35, 2109–2117.

Henry, R.E., Fauske, H.K., 1993. External cooling of a reactor vessel under severe accident conditions. Nucl. Eng. Des. 139, 31–43.

Howard, A.H., Mudawar, I., 1999. Orientation effects on pool boiling critical heat flux (CHF) and modeling of CHF for near-vertical surfaces. Int. J. Heat Mass Transf. 42, 1665–1688.

Ishigai, S., Inoue, K., Kiwaki, Z., Inai, T., 1961. Boiling heat transfer from a flat surface facing downward. In: Proceedings of the International Heat Transfer Conference, Boulder, CO, USA, pp. 224–229.

Katto, Y., 1978. Generalized correlation for critical heat flux of natural convective boiling in confined channels. Trans. JSME 44, 3908–3911 (in Japanese).

Katto, Y., Kosho, Y., 1979. Critical heat flux of saturated natural convection boiling in a space bounded by two horizontal co-axial disks and heated from below. Int. J. Multiphase Flow 5, 219–224.

Kenning, D.B.R., 2004. Optical studies of boiling heat transfer: insights and limitations. Int. J. Heat Fluid Flow 25, 209–222.

Kim, C.S., Suh, K.Y., 2000a. Sensitivity studies on thermal margin of reactor vessel lower head during a core melt accident. J. Korean Nucl. Soc. 32, 376–391.

Kim, Y.H., Suh, K.Y., 2000b. Sensitivity analyses for maximum heat removal from debris in the lower head. J. Korean Nucl. Soc. 32, 392–406.

Kim, Y.H., Suh, K.Y., 2003. One-dimensional critical heat flux concerning surface orientation and gap size effects. Nucl. Eng. Des. 226, 277–292.

Kim, S.H., Baek, W.P., Chang, S.H., 2000. Measurements of critical heat flux for narrow annuli submerged in saturated water. Nucl. Eng. Des. 199, 41–48.

Knudson, D.L., Rempe, J.L., Suh, K.Y., Cheung, F.B., Kim, S.B., 2004. Late-phase melt conditions affecting the potential for in-vessel retention in high power reactors. Nucl. Eng. Des. 230, 133–150.

Lee, S.D., Suh, K.Y., 2003. Natural convection heat transfer in two-dimensional semicircular slice pool. J. Nucl. Sci. Tech. 40, 775–782.

Mayinger, F., 1995. Advanced optical methods. In: Proceedings of the International Conference on Convective Flow Boiling, Banff, Alberta, Canada, pp. 15–28.

Monde, M., Kusuda, H., Uehara, H., 1982. Critical heat flux during natural convective boiling in vertical rectangular channels submerged in saturated liquid. Trans. ASME, J. Heat Transf. 104, 300–303.

Mudawar, I., Howard, A.H., Gersey, C.O., 1997. An analytical model for near-saturated pool boiling critical heat flux on vertical surfaces. Int. J. Heat Mass Transf. 40, 2327–2339.

Nishikawa, K., Fujita, Y., Uchida, S., Ohta, H., 1984. Effect of surface configuration on nucleate boiling heat transfer. Int. J. Heat Mass Transf. 27, 1559–1571.

Rempe, J.L., Knudson, D., Kohriyama T., 2001. Heat transfer between relocated materials and the RPV lower head. In: Proceedings of the Ninth International Conference on Nuclear Engineering (ICONE9), Nice, France.

Rempe, J.L., Suh, K.Y., Cheung, F.B., Kim, S.B., 2004a. Corium retention for high power reactors by an in-vessel core catcher in combination with external reactor vessel cooling. Nucl. Eng. Des. 230, 293–309.

Rempe, J.L., Suh, K.Y., Cheung, F.B., Kim, S.B., 2004b. Conceptual design of an in-vessel core catcher. Nucl. Eng. Des. 230, 311–325.

Rempe, J.L., Knudson, D.L., Condie, K.G., Suh, K.Y., Cheung, F.B., Kim, S.B., 2003. Development of an enhanced in-vessel core catcher for improving in-vessel retention margins. In: Proceedings of the 10th International Topical Meeting on Nuclear Reactor Thermal Hydraulics (NURETH-10), Seoul, Korea, October 5–9, 2003.

Suh, K.Y., Henry, R.E., 1996a. Debris interactions in reactor vessel lower plena during a severe accident—I. Predictive model. Nucl. Eng. Des. 166, 147–163.

Suh, K.Y., Henry, R.E., 1996b. Debris interactions in reactor vessel lower plena during a severe accident—II. Integral analysis. Nucl. Eng. Des. 166, 165–178.

Taylor, J.R., 1982. An Introduction to Error Analysis. University Science Books, Mill Valley, CA, USA, pp. 52–59.

Vishnev, I.P., 1974. Effect of orientating the hot surface with respect to the gravitational field on the critical nucleate boiling of a liquid. J. Eng. Phys. 24, 43–48.

Wolf, J.R., Rempe, J.L., 1993. TMI-2 vessel investigation project integration report, TMI V(93) EG10, Idaho Falls, ID, USA, October.

Xia, C., Hu, W., Guo, Z., 1996. Natural convective boiling in vertical rectangular narrow channels. Exp. Thermal Fluid Sci. 12, 313–324.

Yang, S.H., Baek, W.P., Chang, S.H., 1997. Pool-boiling critical heat flux of water on small plates: Effects of surface orientation and size. Int. Commun. Heat Mass Transf. 24, 1093–1102.

Yoon, H.J., Suh, K.Y., 2000. Two dimensional analysis for the external vessel cooling experiment. J. Korean Nucl. Soc. 32, 407–420.